Practical Implementation of a Neural Network Controller in a Hard Disk Drive

Guido Herrmann, Shuzhi Sam Ge, and Guoxiao Guo

***Abstract*—This brief gives a practical account of the application of an improved adaptive neural network (NN) controller to the voice-coil-motor (VCM)-actuator of a hard disk drive (HDD). Necessary practical modifications are presented which allow the implementation of the controller for a VCM-actuator with high-frequency resonances. For resonance compensation, notch filter compensators are augmented while parameter estimation errors are counteracted by employing robust parameter estimation techniques. It is shown practically that this controller is a good candidate for a track seek/following controller in HDDs.**

***Index Terms*—Actuators, friction, hard disks, neural networks (NNs), servo systems.**

I. Introduction

THE MOST important change in hard disk drive (HDD)-technology has been the rapid increase in data storage density due to the rising demand in data storage systems. Thus, high-performance servo controllers are needed, as data are accessed via the electro-mechanical voice-coil-motor (VCM)-actuator. The servo system places the actuator tip, holding a read/write head, over one of the circular concentric data tracks written on the rotating disk.

For HDD servo control, two different control problems have to be considered: seek/settling and track following. Seek/settling control has to ensure a fast change of the read/write head from one track to another. For track following, high-bandwidth controllers are necessary to ensure good error rejection capabilities while counteracting disturbances. For many years, the proximate time-optimal servo controller (PTOS) [4] has been a suitable solution for both issues. However, continued demand on closed-loop performance made it necessary to employ different control techniques for seeking, settling [25] and tracking [7], [13] using gain scheduling methods. In contrast, a single adaptive controller is presented in this brief which is also capable of dealing with friction disturbances.

Compensation of bias-forces such as friction has attracted significant interest among HDD servo control engineers, as higher data density demands a more precise head positioning accuracy. Techniques for compensation of pivot friction have been suggested by many researchers [3], [11]. For instance, a high-order large-scale multilayer fuzzy-controller was used in [10] to estimate the bias force prior to the actual control process. It has been acknowledged that the modeling task for friction is complex [8], [17], [21]. In actual fact for high-precision servo control systems, it is necessary to investigate friction in smaller dimensions, leading to complex continuous static or dynamic models on the micro-level which depend on both position and velocity of the actuator [2], [22].

Motivated by the need to tackle these discussed issues in HDD-servo control, adaptive neural network (NN) techniques developed for nonlinear systems [5], [14], are an attractive alternative to existing methods. Such adaptive control structures are a significant advancement of adaptive controllers by [18] and [19]: NN-estimation allows the modeling of a much larger class of nonlinear functions, including the highly nonlinear friction. Hence, inspired by the work of [5] and [22], a nonlinear NN controller is proposed incorporating an estimator for the VCM-actuator mass/inertia and an NN-based control element counteracting disturbances such as friction. In contrast to prior work, the linear control element is augmented by a differential element (D) to obtain the common flexibility of a PID-controller for HDD-servo control.

The benefits of adaptive techniques in HDD-servo systems have been already practically investigated in [9], [12], [15], and [16]. For instance, adaptive controllers were used for cancellation of actuator resonances, achieving subsequently the increase of the servo bandwidth [23], [24]. The importance of resonance cancellation was discussed in [24]. This importance has been acknowledged in this brief by considering simple notch filtering techniques [13].

Hence, this brief presents an improved NN control algorithm in application to a HDD-servo system. Practical techniques such as those for resonance cancellation and for robustification of the parameter estimation algorithms are provided, followed by a concise description of various experimental results.

II. Adaptive Controller With Bias-Force Compensation

For the theoretical development, consider the double integrator model representing the VCM-actuator with control input u as follows:

$$M\ddot{q} + F = u \tag{1}$$

where the scalar q is the position of the VCM-actuator tip, M the unknown system constant, which models the system inertia/mass, while the function F represents bias-forces due to static pivot, bearing friction or due to the VCM-flex-cable. Note that both the equivalent moment of inertia M and the bias force F are scaled in practice by input and output gains. For reasons of simplicity, high-frequency flexibilities of VCM-actuators are not explicitly considered here.

Manuscript received October 29, 2003. Manuscript received in final form May 17, 2004. Recommended by Associate Editor N. Sundarajan. This work was completed during a two year Senior Research Fellowship of G. Herrmann at the A*STAR Data Storage Institute, Singapore.

G. Herrmann is with the Department of Engineering, University of Leicester, Leicester, LE1 7RH, U.K. (e-mail: Guido_HERRMANN@ieee.org).

S. S. Ge is with the Department of Electrical and Computer Engineering, National University of Singapore, Singapore 119260 (e-mail: elegesz@nus.edu.sg).

G. Guo is with the A*STAR Data Storage Institute, Singapore 117608 (e-mail: GUO_Guoxiao@dsi.a-star.edu.sg).

Digital Object Identifier 10.1109/TCST.2004.838567

It can be assumed that $|F| < K_F$ is bounded. As discussed in Section I, the function F can be regarded as a continuous function of position q and velocity $\dot{q}$

$$F(q,\dot{q}) : D \rightarrow [-K_F, K_F]. \tag{2}$$

$D \subset \mathbb{R}^2$ is a compact set, representing the bounded operation area of the VCM-actuator. It has been shown that NN radial basis functions $\phi_i \geq 0, \phi \in \mathbb{R}^m$, can be used to approximate arbitrarily closely any continuous function in a compact set so that

$$F(q,\dot{q}) = \theta^T \phi + E_F \quad \theta, \phi \in \mathbb{R}^m \quad E_F \in \mathbb{R} \tag{3}$$

for a large enough number $m > 0, m \in \mathbb{N}$, of NN nodes. Each radial basis function ϕ_i is weighted via a respective element θ_i of the neural weight vector $\theta \in \mathbb{R}^m$. The modeling error E_F is bounded, $|E_F| < K_E$. The bound K_E decreases with increasing value of m and more accurate choice of the radial basis function parameters. For this work, each NN node comprises of a *Gaussian* radial basis function $\phi_i(q,\dot{q}), \phi = [\phi_1 \ \cdots \ \phi_m]^T$

$$\phi_i(q,\dot{q}) = \exp - \frac{(q - c_{q/i})^2 + (\dot{q} - c_{\dot{q}/i})^2}{\sigma_i^2}. \tag{4}$$

The values of $\sigma_i \in \mathbb{R}^+$ and $c_{q/i}, c_{\dot{q}/i} \in \mathbb{R}$, are the variance and center positions of the Gaussian radial basis functions.

For demand tracking, the desired trajectory is given by the bounded values of the position q_d and the desired velocity $\dot{q}_d$ and acceleration $\ddot{q}_d$. For control, the following signals are used:

$$\begin{aligned} &\epsilon = q - q_d, \quad \dot{q}_r = \dot{q}_d - \lambda\epsilon \\ &r = \dot{q} - \dot{q}_r = \dot{\epsilon} + \lambda\epsilon, \quad \lambda > 0. \end{aligned} \tag{5}$$

From this, the estimates, $\hat{M}$ and $\hat{\theta}$, for the equivalent moment of inertia M and the neural weights θ are

$$\dot{\hat{M}} = -\gamma \ddot{q}_r r, \quad \dot{\hat{\theta}} = -\Gamma \phi(q,\dot{q}) r \tag{6}$$

where a learning coefficient $\gamma > 0$ and a positive definite learning coefficient matrix $\Gamma \in \mathbb{R}^{m \times m}, \Gamma = \Gamma^T$ are used.

Employing ideas from [22], it can be shown that the VCM-actuator-system is robustly stabilized by the tracking control law

$$\begin{aligned} u = &\underbrace{\hat{M}\ddot{q}_r}_{=u_I} + \underbrace{\hat{\theta}^T \phi(q,\dot{q})}_{=u_B} - \underbrace{\left(K_d \dot{r} + Kr + K_i \int_0^t r d\tau \right)}_{=u_L} \\ &- \underbrace{K_E \mathrm{sgn}(r)}_{=u_S} \\ K \in \mathbb{R}^+ \quad &K_i \geq 0, \quad K_d > -M \end{aligned} \tag{7}$$

so that the *tracking error ϵ converges to zero* despite the constant bounded bias force disturbance F. However, it is important to understand from [22] that *the estimation errors $M - \hat{M}$ and $\theta - \hat{\theta}$ remain bounded* only. Hence, convergence of the estimates $\hat{M}$ and $\hat{\theta}$ to the true physical value is not ensured.

The term u_B in (7) is introduced to compensate for bias-forces and u_I is used to improve tracking despite a slowly changing or unknown value of M. The sliding mode term $u_S = K_E \mathrm{sgn}(r)$ has been introduced to compensate robustly for the modeling error E_F (3).

The linear control term, u_L, extends the control law of [5], [22] by the differential term $K_d \dot{r}$ creating the full flexibility of a PID-control element for the adaptive control strategy. It will be discussed later that the D-element has proved to be beneficial. However, note that the D-element employs an acceleration signal $\ddot{q}$. Nevertheless, reliable estimates could be obtained for this, since accurate laser measurement technology was used to obtain practically the actuator position q. Further note that the approach of acceleration estimation is not uncommon for practical systems [20].

III. Practical Implementation of the NN-Controller

Some practical issues have not been considered in the theoretical foundation for the NN-control scheme of Section II, such as practical actuator resonance compensation and robust parameter estimation algorithms to suppress high-frequency resonances and windup of the estimation algorithms. Considering those, the schematic from Fig. 1 is a representation of the closed-loop system, for which a detailed description will be given next.

A. Sliding Mode Control Term u_S

A practical problem of sliding mode control is chattering of the control signal which is caused by high-frequency switching along the sliding mode plane $r = 0$. To prevent chattering, a commonly known technique [5, pp. 113] is to exchange the signum-function, $\mathrm{sgn}(r)$, with the saturation-function

$$\mathrm{sat}(r/d_s) = \begin{cases} 1, & r > d_s \\ -1, & r < -d_s \\ r/d_s, & \text{otherwise} \end{cases}$$

for $d_s > 0$. This introduces a boundary layer around $r = 0$ for which the layer width decreases with d_s.

It is readily understood that $|E_F|$ is constant bounded. However, as E_F is a residual part of the bias force disturbance $F(q,\dot{q})$ (3), it can be implied from (2) and [6], that E_F is a very complex nonlinear function of displacement q and velocity $\dot{q}$. It is readily understood from [6] that viscosity friction causes significant dependence of the friction force on velocity $\dot{q}$. In contrast, stiction can depend on displacement q [6]. Hence, for sufficiently small bound $K_E > |E_F|$, i.e., small q and $\dot{q}$, it is permissible to consider for $|E_F|$ the following parametric-type bound:

$$|E_F| \leq K_{s1} + K_{s2}|q| + K_{s3}|\dot{q}| \tag{8}$$

for $0 \leq K_{s1} \leq K_E$ and $K_{s2}, K_{s3} \geq 0$. This relaxes the bound K_E for small values of $|q|$ and $|\dot{q}|$. Thus, it is advisable to modify the sliding mode term according to suggestions of [1], [5]:

$$u_S = (K_{s1} + K_{s2}|q| + K_{s3}|\dot{q}|)\mathrm{sat}(r/d_s) \tag{9}$$

which can decrease control effort for small values of $|q|$ and $|\dot{q}|$.

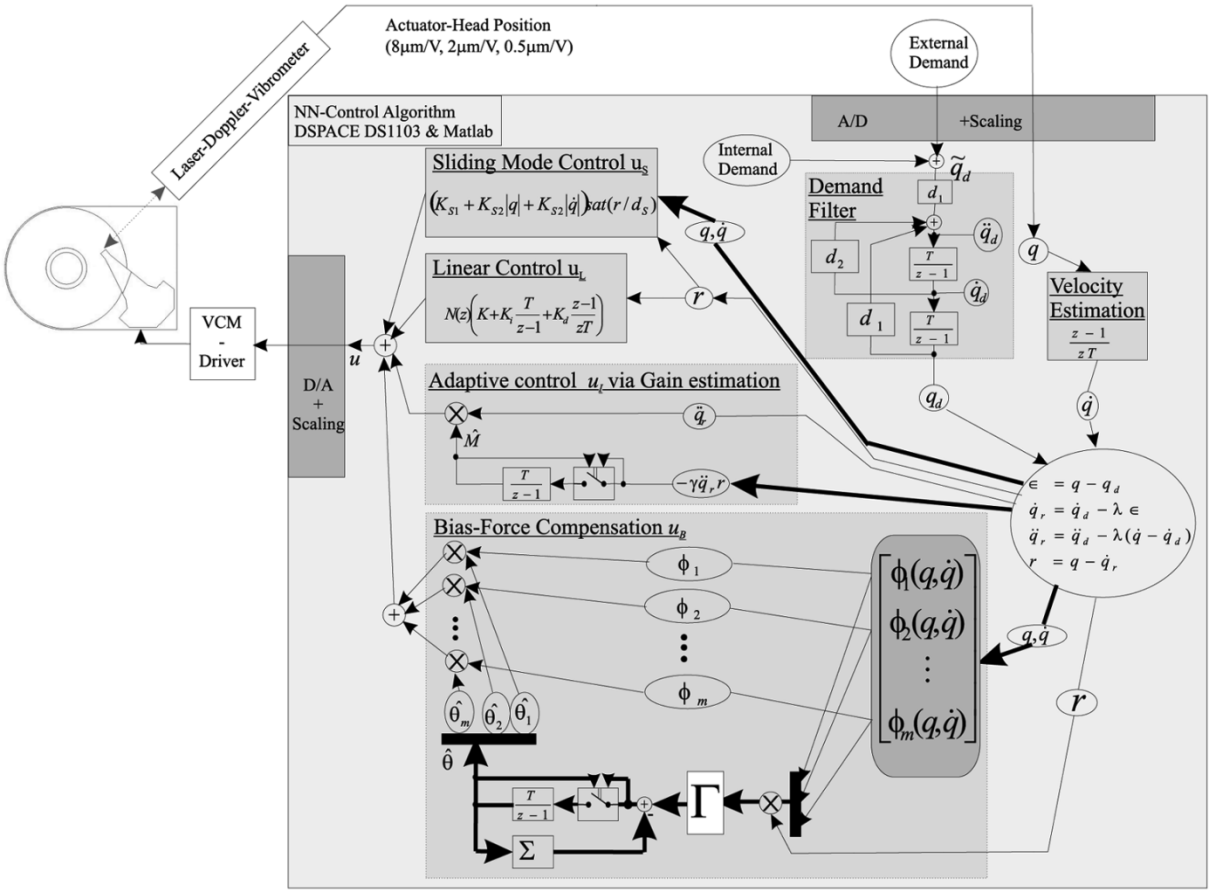

Fig. 1. Schematic of the controller setup for the HDD.

B. Boundedness of $\hat{M}$ and $\hat{\theta}$ for the Adapting Control Terms u_I and u_B

The estimation algorithms of (6) are known to be sensitive to bounded disturbances. Hence, the introduction of the smoothed sliding-mode control term of (9) may lead to the unbounded growth of the estimates (6), [5], [22]. Hence, similar to [5, pp. 120], robust parameter estimation techniques have to be used. Note that it is physically not possible for M to be nonpositive, $M \not\leq 0$. Furthermore, it seems to be practical to assume the knowledge of a reasonably large bound $\bar{M}$ for M

$$M < \bar{M} \quad \hat{M} < \bar{M}$$

while the bias-force F is limited to $[-K_F, K_F]$. Thus, the estimation algorithms should be "switched off" once these limits are reached. For the bias-force estimate $\hat{F}$, this can be done indirectly by limiting each element $\hat{\theta}_i \in [-\bar{K}_F, \bar{K}_F]$. In addition, the robust σ-modification scheme [5, pp. 120] is used for the bias-force estimator

$$\dot{\hat{\theta}}_i = \begin{cases} 0, & \begin{array}{c}(\hat{\theta}_i \geq \bar{K}_F \text{ and } \mathcal{E}_{\theta,i} > 0) \\ \text{or} \\ (\hat{\theta}_i \leq -\bar{K}_F \text{ and } \underbrace{\Gamma_i \phi(q,\dot{q}) r - \Sigma_i \hat{\theta}}_{=\mathcal{E}_{\theta,i}} < 0)\end{array} \\ \mathcal{E}_{\theta,i}, & \text{otherwise} \end{cases} \tag{10}$$

for which the positive semidefinite matrix $\Sigma = [\Sigma_1^T \ \Sigma_2^T \ \cdots \ \Sigma_m^T]^T \in \mathbb{R}^{m\times m}$ and the positive definite learning coefficient matrix $\Gamma = [\Gamma_1^T \ \Gamma_2^T \ \cdots \ \Gamma_m^T]^T \in \mathbb{R}^{m\times m}$ are employed, with Σ_i and Γ_i compatibly dimensioned. However, the σ-modification did not prove to be useful for the system inertia estimator, so that the following scheme is used only:

$$\dot{\hat{M}} = \begin{cases} 0, & \begin{array}{c}(\hat{M} \leq 0 \text{ and } -\gamma \ddot{q}_r r < 0) \\ \text{or} \\ (\hat{M} \geq \bar{M} \text{ and } -\gamma \ddot{q}_r r > 0)\end{array} \\ -\gamma \ddot{q}_r r, & \text{otherwise} \end{cases}. \tag{11}$$

C. Linear Control Term u_L

For control engineers in HDD-servo control, it is common to cancel high-frequency resonances with notch filters [13]. This allows for the consideration of a controller design in two frequency ranges. The lower frequency range is dominated by the characteristics of the neural-network controller. In contrast, the higher frequency range is mainly influenced by the characteristics of the linear control element. For this reason, it must be noted that notch filters can introduce a significant phase shift. Assuming that the VCM-actuator is set in series with the notch filter, the phase shift can distort the double integrator characteristics of the actuator leading to wrong estimates for the values of $\hat{M}$ and $\hat{F}$. Hence, it seems to be more feasible to implement the notch filter directly together with the linear control term only.

Assuming $R(s)$ and $N(s)$ to be the Laplace transform of r and the notch filter, the linear control term incorporating the notch filter can be written in the s-domain as

$$u_L = \left(K + K_i \frac{1}{s} + K_d s \right) N(s) R(s). \tag{12}$$

D. Controller Discretization

Since DSP-technology is chosen for implementation, the continuous control algorithm has to be discretized: A sufficiently fast sampling frequency has to be used to retain certain controller characteristics as those of differentiators and integrators. Integrators are replaced by the Forward-Euler integration method for which the transfer function in the z-plane is $(T)/(z-1)$, where T is the sampling time. Numeric differentiation is carried out via $(z-1)/(zT)$. In particular, the velocity and the acceleration of the VCM-actuator tip are estimated from the position measurement using this differentiation method (Fig. 1). Note that it is not uncommon to incorporate an acceleration estimate into a practical control scheme as it has been documented in [20]. The beneficial value in doing so will be discussed for the controller design.

E. Demand Trajectory Filter

To create the necessary demand trajectory $q_d, \dot{q}_d$, and $\ddot{q}_d$, a demand input filter is designed using a second-order filter (Fig. 1). It is easily verified, that the filter approximates a continuous second-order filter with poles only at $-(d_2)/(2) \pm \sqrt{(d_2^2)/(4) - d_1}$.

IV. Controller Design

The NN-control scheme suitably adapted for an actuator with high-frequency flexibilities is now exemplified on an actual HDD-plant. For this, a VCM-actuator with read/write head suspension but without slider and read/write head is used. The position of the VCM-actuator tip is determined by a Laser-Doppler-Scanning-Vibrometer[1] (LDV) at three different measurement sensitivities of 8, 2, and 0.5 μm/V for optimal measurement range. The casing of a commercially available hard-disk drive has been partially cut to allow for the laser to measure the VCM-actuator tip position (Fig. 2). Since the HDD-casing has not been fully removed, the windage and spindle vibrations created by the rotating disk are a realistic disturbance.

A Dynamic Signal Analyzer[2] (DSA) in the 'Swept-Sine-Signal'-mode has been used at two different excitation amplitudes to measure the VCM-actuator in closed loop. This approach shows the effects of friction below 250 Hz since the frequency response amplitudes differ for different excitation amplitudes. Further, note that the VCM-plant has three significant resonances at 3.45, 5.2, and 8.1 kHz (Fig. 3).

For controller implementation, a DSP-based system,[3] is used employing a sampling frequency of $1/T = 20$ kHz (Fig. 1).

[1]Polytec OFV 3001S, Polytec, Waldbronn, Germany.

[2]HP 35 670A, Hewlett Packard Company, Washington.

[3]DSpace DS1103 is a product of dSPACE GmbH, Paderborn, Germany.

Fig. 2. Experimental setup. HDD (left), LDV-laser unit (left), VCM-driver (center-left), LDV-control-unit (PC right).

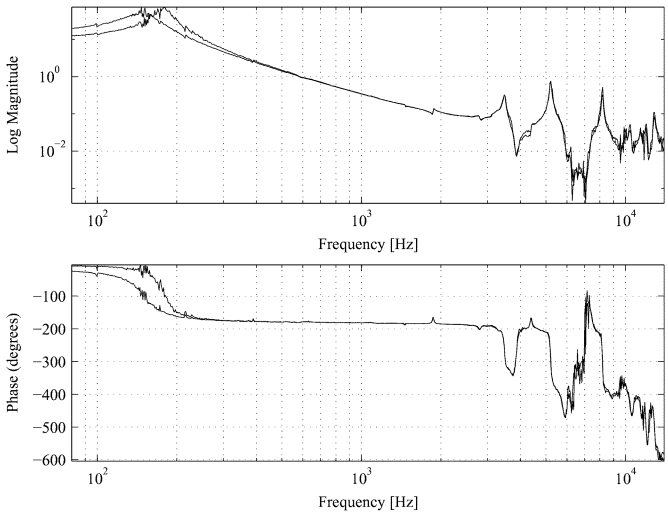

Fig. 3. Frequency response of the VCM-plant incorporating the voltage-to-current driver, LDV-measurement at 8 μm/V.

The practically evaluated controller bandwidth will not exceed 2 kHz and the largest considered actuator resonance is 8.1 kHz. Hence, the sampling frequency should be sufficiently fast for implementation of the continuous control scheme. Due to this fast-sampling approach, the ultimate performance result of the adaptive controller will depend primarily on a good on-line design.

To simplify the subsequent selection of parameters of the nonlinear control system terms, the overall VCM-measurement and the DSP-control signal have been scaled[4] by S_{meas} and S_{contr}:

$$S_{\text{meas}} = 2 \cdot 10^{-3} \times \begin{pmatrix} \underbrace{1}_{\text{LDV=8 } \mu\text{m/V}} & \underbrace{1/4}_{\text{LDV=2 } \mu\text{m/V}} & \underbrace{1/16}_{\text{LDV=0.5 } \mu\text{m/V}} \end{pmatrix}$$
$$S_{\text{contr}} = 2.6 \cdot 10^{-6}. \tag{13}$$

Note that this procedure introduces also a scaling of the estimates $\hat{M}$ and $\hat{F} = \hat{\theta}^T \phi$.

The controller design follows the same succession of steps as presented below.

[4]The scaling factors include the scaling of $1/10$ and 10 for measurement/control in the DSP-system.

A. Design of a Demand Trajectory Filter

The demand trajectory filter was tuned to ensure a closed-loop settling time of about 1 ms, so that $d_1 = 20\,500\,000$ and $d_2 = 9000$ (Fig. 1).

B. Design of the Linear Controller Term u_L

The first step is to choose $\lambda = 10$ (5). Then, an eighth-order notch filter $N(z)$ (12) is designed cancelling the three significant resonances via three second-order notch filters. Furthermore, the filter $N(z)$ introduces a second-order low pass with a bandwidth of about 9 kHz. Afterwards, the PID-elements of the linear control term can be adjusted to the gains $K = 84616$, $K_i = 225\,000\,000$, and $K_d = 4$. Guidelines for high-performance designs are given in [13]. The gain K_d for the differential element reduces overshoots and improves high-frequency closed-loop performance. For this, an estimate for the acceleration $\ddot{q}$ has been reliably derived from the high-quality LDV-measurement q.

C. Design of the Adaptive Controller Term u_I

The inertia compensation term u_I has mainly a positive effect on the tracking performance of demand signals in the frequency range above 150 Hz and below 1.4 kHz. For controller adjustments, a periodic square wave signal of about 100 Hz is suitable for the demand $\tilde{q}_d$ as it can be regarded as a broadband signal but also allows adaptation due to periodicity. The value of $\gamma = 1$ was chosen by gradually increasing and evaluating tracking performance. Adaptation is found to be fast. The value of $\bar{M} = 10.5$ from the algorithm in (11) was tuned by gradually decreasing $\bar{M}$ from a large value. When evaluating performance, saturation of $\hat{M}$ at the upper limit $\bar{M}$ was accepted for short periods only. For initialization of the algorithm (11), the boundary $\hat{M}(t=0) = \bar{M} = 10.5$ should be used as it allows fast convergence.

D. Design of the Adaptive Controller Term u_B

A maximal amount of $m = 11$ neural-network nodes has been chosen: The effectiveness of the NN term u_B appeared to improve only marginally when increasing the number of NN-nodes any further. Thus, performance was deemed sufficient for this amount of NN-nodes. Moreover, this choice allows for a good comparative performance investigation of the controller with different numbers of $m \leq 11$. Furthermore, it was aimed to remain below the possible performance limits of the implementation equipment to retain good controller handling qualities during experimentation.

The values of $c_q, c_{\dot{q}}$, and σ_i for the Gaussian radial basis functions $\phi_i(q, \dot{q})$ (4) have to be carefully chosen so that they cover the operational range of the controller. It is of significance to model for the bias force the whole dynamic range of demanded responses with the NN-approach. In this sense, good parameter choices for each NN-node can retain a low number of NN-nodes. However, it is not important to select the NN-parameters with an accuracy higher than 10%.

It is important to note that a good result for bias force compensation was mainly due to a good model incorporating the velocity $\dot{q}$. Thus, the parameters $c_q, c_{\dot{q}}$, and σ_i for the first five NN-nodes (Table I) were chosen to cater for a respective large range of velocities. For this, dynamic responses of large position amplitudes up to 4 μm were observed. The maximal values of the velocity $\dot{q}$ were determined during the experiment and accordingly the center values $c_{\dot{q}}$ were distributed over the interval $[-7, 7]$, while retaining a large variance $\sigma_i = 10$ for this large range of velocities.

TABLE I
BIAS-FORCE ESTIMATOR CHARACTERISTICS

Controller features:	c_q	$c_{\dot{q}}$	σ	diag(Σ)	diag(Γ)
1	-0.002	-7	10	$12 \cdot 10^6$	5
2	-0.001	-3	10	$12 \cdot 10^6$	5
3	0	0	10	$12 \cdot 10^6$	5
4	0.001	3	10	$12 \cdot 10^6$	5
5	0.002	7	10	$12 \cdot 10^6$	5
6	$4 \cdot 10^{-5}$	0.3	$1/\sqrt{6}$	$8 \cdot 10^5$	20
7	$-4 \cdot 10^{-5}$	-0.3	$1/\sqrt{6}$	$8 \cdot 10^5$	20
8	0.0002	1	1	$5 \cdot 10^6$	80
9	-0.0002	-1	1	$5 \cdot 10^6$	80
10	0	0.05	$1/\sqrt{10}$	$8 \cdot 10^5$	5
11	0	-0.05	$1/\sqrt{10}$	$8 \cdot 10^5$	5

The parameters for the sixth and seventh node (Table I) consider an actuator close to the demanded set-point with small velocity. Hence, center values and variances are chosen small. In particular, the variance $\sigma_i < 1$ and the velocity center value $c_{\dot{q}_i} < 1$ were chosen small.

The last four values of $c_q, c_{\dot{q}}$, and σ_i from Table I have been chosen to model bias and friction forces for the dynamics in response to a demand amplitude range below 0.5 μm. Thus, the parameters $\sigma_i \leq 1$ and $c_{\dot{q}_i} \leq 1$ are limited according to the observed velocity values in this demand range.

The σ-modification values from the diagonal matrix Σ of (10) were kept large enough to retain the estimated bias-force, $\hat{F}$, bounded while achieving acceptable performance (see Table I for diagonal elements diag(Σ)). In the same way, the limiting value, $\bar{K}_F = 10\,000$, for the neural weight estimates $\hat{\theta}$ was chosen small enough to retain stability and fast convergence. Similarly, the values of the diagonal learning coefficient matrix, Γ, were not chosen too large (Table I).

E. Design of the Sliding Mode Term u_S

The sliding mode term parameters from (9), $K_{s1} = 1, K_{s2} = 1, K_{s3} = 1$, and $d_s = 100$, were tuned so that the linear control and the adaptive control terms dominate the overall closed-loop performance.

V. EXPERIMENTAL RESULTS

For controller assessment, three different classes of results are discussed: tracking of sinusoidal demands, track seeking and track following when affected by windage and vibrational disturbances.

A. Tracking for Sinusoidal Demands

An approach to evaluate the tracking capabilities of a controller is to conduct a frequency response analysis. This can be accomplished by using a DSA in the "Swept-Sine-Signal"-mode. Hence, the demand signal $\tilde{q}_d$ from Fig. 1 and Section III-E is created by a sinusoidal signal for which the

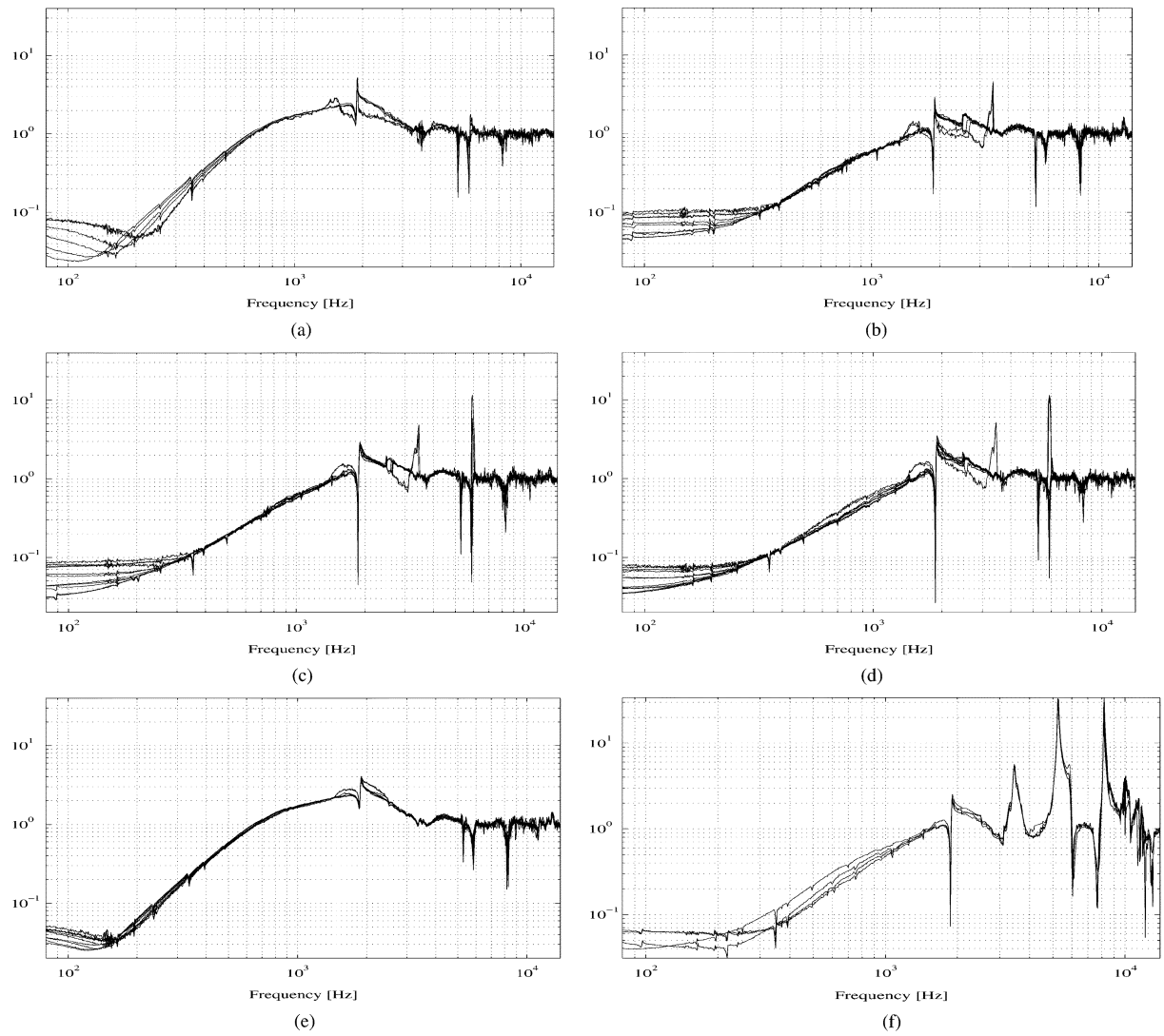

Fig. 4. Frequency characteristics for error rejection analysis of controller. (a) Linear controller only and $\hat{M} = 0, \hat{\theta} = 0$. (b) With $\hat{M}$ estimation; without $\hat{F}$ estimation ($\hat{\theta} = 0$). (c) With $\hat{M}$ estimation and 7-node $\hat{M}$ estimation. (d) With $\hat{M}$ estimation and ll-node $\hat{F}$ estimation. (e) 11-node $\hat{M}$ estimation; without inertia adapt., $\hat{M} = 0$. (f) Values fixed $\hat{M} = \text{const.} \neq 0$ and $\hat{\theta} = \text{const.} \neq 0$.

frequency is gradually increased from small to high frequencies. The frequency response characteristics from q_d to ϵ (5) can be evaluated. This procedure is common when evaluating linear control systems. However, neural-network controllers are inherently nonlinear controllers. Hence, the practically measured frequency response analysis cannot be understood in terms of linear systems analysis. Nevertheless, this approach can give an insight into the error rejection capabilities of the controller for sinusoidal demands.

When analysing each controller configuration, the DSA-measurements have been conducted for demand signals $\tilde{q}_d$ with five different amplitudes, 0.1, 0.25, 0.4, 0.7, and 1 μm. Abusing normal convention, terms known from linear control such as sensitivity bandwidth are used in the following analysis.

1) Control Element u_I: Activating the adaptive control term u_I together with the linear control term has the effect of increasing significantly the sensitivity bandwidth from an initial value of 629 Hz for the linear controller to 1.4 kHz [Table II and Fig. 4(a), (b)]. In terms of linear control, the value for the sensitivity bandwidth of 1.4 kHz could be regarded as a significant achievement. Control engineers usually design VCM-servo controllers with an open-loop bandwidth which is approximately a third of the first significant actuator resonance [13], i.e., about 1.1 kHz in this case.

TABLE II
WORST CASE FREQUENCY RESPONSE CHARACTERISTICS FOR ERROR REJECTION

Controller features		rejection below 100 Hz [db]	Bandwidth [kHz]	rejection at 1.9 KHz [db]
$\hat{M}$	$\hat{\theta}$			
=0 (linear cont.)	=0 (linear cont.)	-21.5	0.629	14.4
$\neq$0 (adap. active)	=0 (inactive)	-19.7	1.4	9.3
$\neq$0 (adap. active)	$\neq$0 (5 nodes, active)	-20.5	1.21	11.1
$\neq$0 (adap. active)	$\neq$0 (7 nodes, active)	-21.1	1.39	9.39
$\neq$0 (adap. active)	$\neq$0 (11 nodes, active)	-22	1.39	10.7
= 0 (inactive)	$\neq$0 (11 nodes, active)	-26	0.639	12.2
= const. (value fixed)	= const. (value fixed)	-23	1.55	8.03

For small demand frequency of ≈100 Hz, the control term u_I degrades the performance of the initially linear controller resulting in a loss of approximately 2 dB error rejection capability.

2) Bias-Force Compensator u_B: The loss of low-frequency error rejection due to the system inertia estimator of u_I is compensated when enabling the control element u_B [Table II and Fig. 4(c)–(d)]. Low-frequency error rejection improves by more than 2.5 dB when increasing the NN model order from $m = 5$ to $m = 11$ nodes. Note that the low-frequency region is where generally the effect of friction acts deteriorating for a practically measured frequency response.

The bias-force compensator u_B activated together with the linear controller only improves the low-frequency sensitivity response by more than 4 dB compared to the linear controller [Fig. 4(a), (e) and Table II].

3) Sensitivity Response Peaks at High and Medium Frequency: The bias-force and the system inertia estimator can improve error rejection at high frequency. This has been observed in Table II for the sensitivity peak at 1.9 kHz. This peak coincides with a small VCM-resonance (Fig. 4).

For some high-frequency sinusoidal demands, the system inertia estimation algorithm fails which can lead to sudden jumps of $\hat{M}$ between the two extrema 0 and $\bar{M}$ (11). These jumps coincide with the peaks at 3.45 kHz and 5.9 kHz of the sensitivity characteristics of Fig. 4(b)–(d). Only one of these two peaks is in the proximity of an actuator resonance. This phenomenon is not necessarily always repeatable for a particular controller configuration. Thus, these peaks are spurious and practically irrelevant since demand signals in HDD-servo systems are generally bandlimited to frequencies below 2 kHz.

4) Controller Configuration With Fixed Adapted Parameters: It has been found that it is not advisable to fix in particular the estimated system inertia, $\hat{M}$. The fixed value $\hat{M}$ introduces a linear control term $\hat{M}\ddot{q}_r$ into the control law of (7). This procedure increases the high-frequency controller gain and leads to the excitation of high frequency modes [Fig. 4(a)].

B. Track Seeking Performance

Two different aspects are evaluated: The first aspect considers the improvement of demand following performance due to both adaptive control terms u_I and u_B, while the effect of u_B as bias-force compensator is investigated afterwards:

1) Small and Medium Step Demands: Linear Versus Adaptive: Due to the adaptive structure of the control method, the NN-controller shows good demand tracking characteristics. For a demand step of 8 μm [Fig. 5(a)] and 0.2 μm, an overshoot of approximately 15% is noted for the linear controller while with controller adaptation the demand is tightly followed. From Fig. 5(b), it is seen that the estimate $\hat{M}$ quickly settles back to lower values between 10 and 10.5 after a short time of saturation. This shows the advantage of limiting the estimated value since it shortens the transition period introduced by the demand step.

The step response characteristics of Fig. 5(a) have been taken from a time series with $\tilde{q}_d$ being a square wave signal of constant period. However, the good tracking performance of the adaptive controller is also confirmed when considering random step demands with a maximal switching frequency of 80 Hz (Fig. 6). It

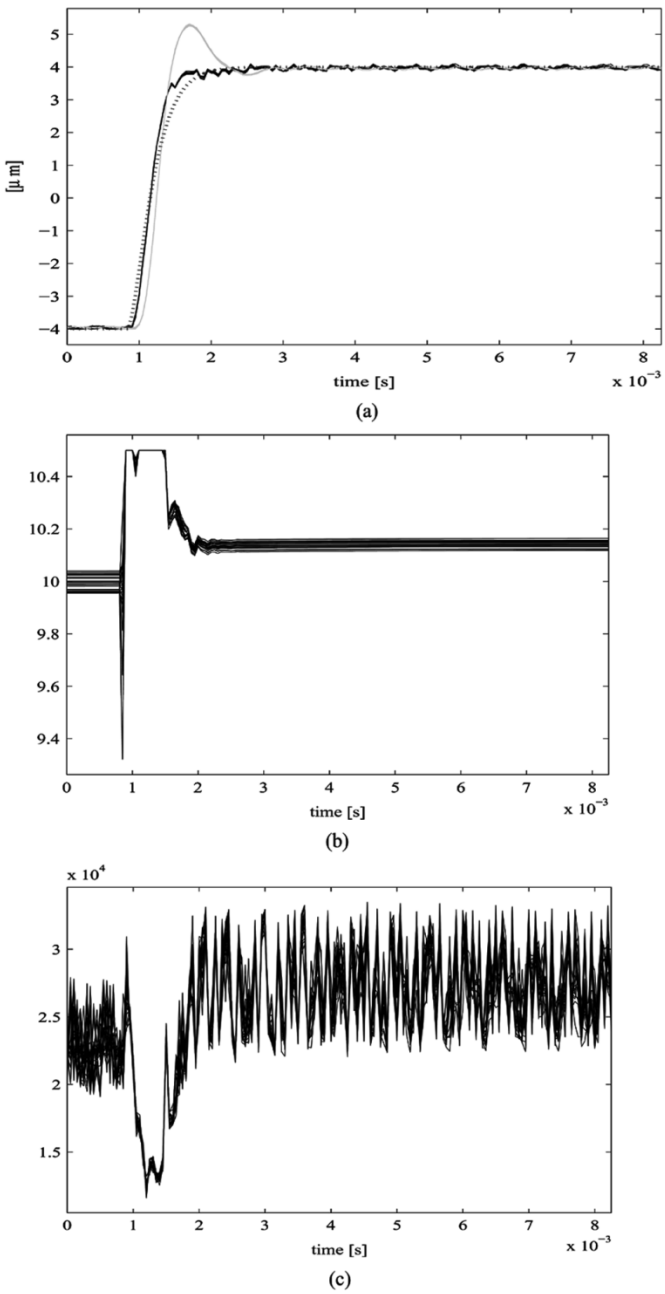

Fig. 5. Several recorded step responses (≥ 25) for control with both estimators enabled (11 nodes) and for $\hat{M} = 0, \hat{\theta} = 0$. (a) Output measurement: $dashed$ = demand q_d, black line = with adaptation, light line: without adaptation. (b) $\hat{M}$ estimate for adaptive controller. (c) $\hat{F}$ estimate for adaptive controller.

is also obvious that both estimates $\hat{M}$ and $\hat{F}$ [Fig. 6(b) and (c)] do not necessarily settle at the same value as for the periodic demand signal [Fig. 5(b) and (c)]. As emphasized in Section II, the estimates are not ensured to converge to their true values. Hence, for this reason, the positive effect of the adaptation algorithm on the closed system has been evaluated, rather than the significance of $\hat{M}$ and $\hat{F}$ as an estimate for a physical value.

2) Bias-Force Compensator u_B: Step demand responses of 1 μm are compared considering the controller without any estimator, $\hat{\theta} = 0, \hat{M} = 0$, and with a bias-force estimator of $m = 11$ nodes. From Fig. 7, the settling time is smaller for the controller with enabled bias-force estimator. Most importantly,

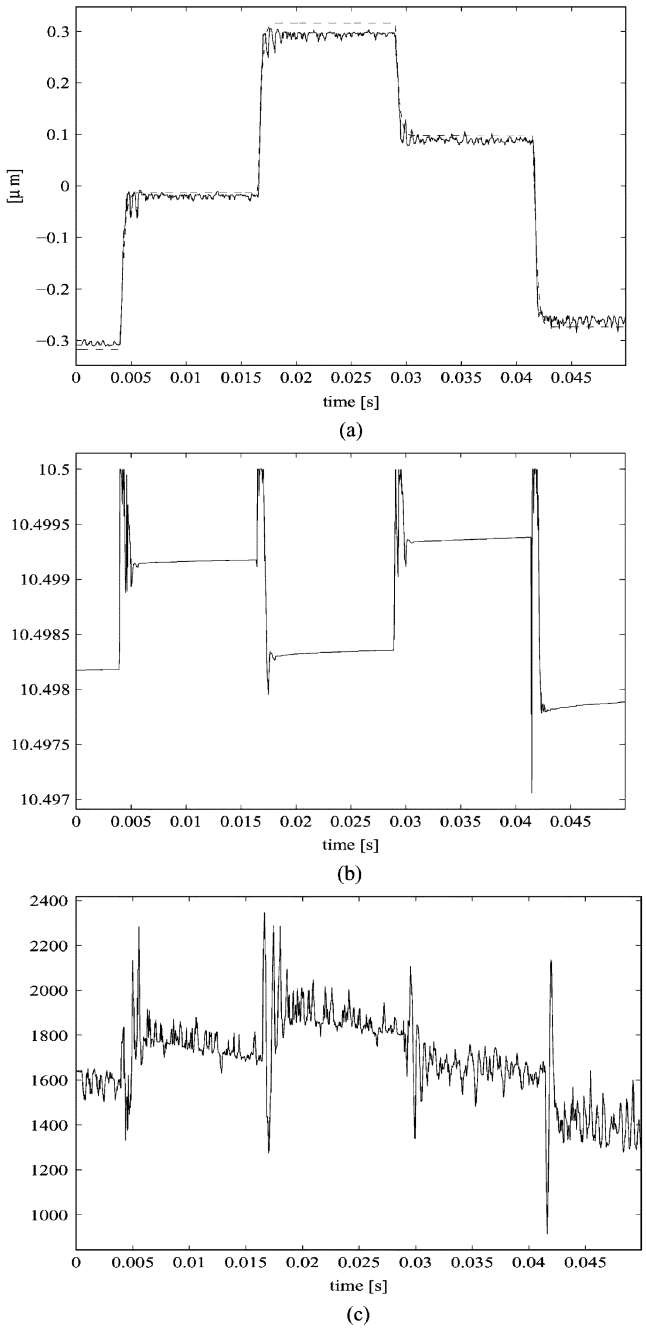

Fig. 6. Random step response characteristics, with adaptation of $\hat{M}$ and $\hat{\theta}$ (11 nodes). (a) Output measurement. $dashed$ = filtered demand q_d, line = with adaptation. (b) Estimate $\hat{M}$. (c) Estimate $\hat{F} = \hat{\theta}^T \phi$.

the magnified image of the tracking error from Fig. 7(b) shows that the steady-state position error $q - q_d$ has improved for the controller with bias-force compensator.

C. Track Following Performance

In HDD-servo systems, track following $(\tilde{q}_d = 0)$ is also a significant task. Disturbance rejection is important in this case. Hence, windage and spindle vibrations are introduced via rotating disks at a rotational spindle speed of 5000 r.p.m.. For this reason, the adaptive NN-controller considering the system inertia estimator and an $m = 11$-node bias-force compensator is investigated as well as the controller for $\hat{\theta} = 0, \hat{M} = 0$. Time

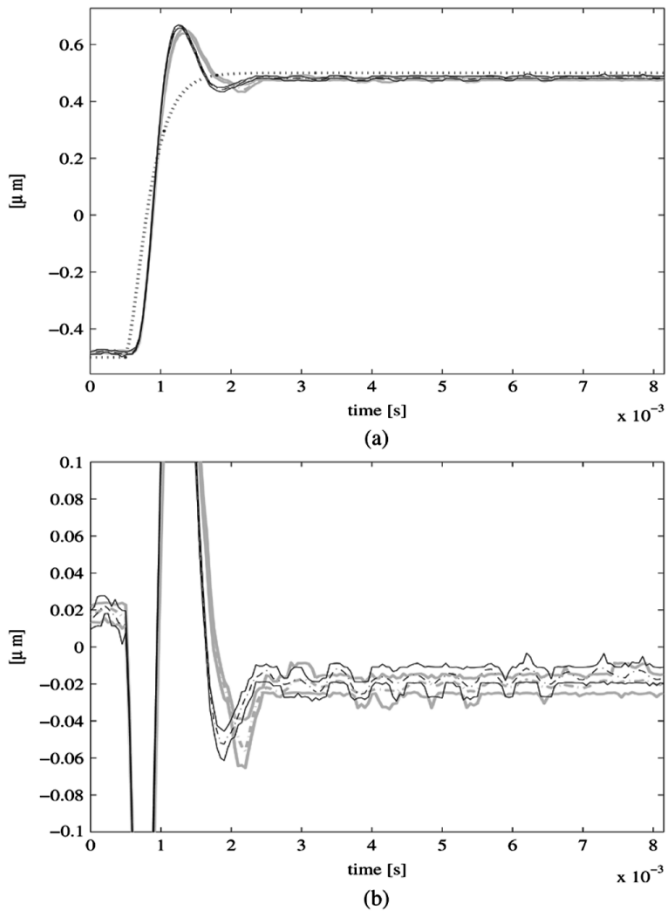

Fig. 7. Data envelope for several recorded step responses (≥ 25) considering control with $\hat{F}$-estimation (11 nodes) and for $\hat{M} = 0, \hat{\theta} = 0$. (a) Output measurement. $dashed$ = demand q_d, black = with adaptation, light = without adaptation (line = envelope, dot-dashed = mean). (b) *Magnified* tracking error. black = with adaptation, light = without adaptation (line = envelope, dot-dashed = mean).

response data have been sampled at 20 kHz for a period of one second obtaining 20 000 data points for statistical evaluation. The standard deviation of the position error signal $q - \tilde{q}_d = q$ for the adaptive controller is $\sigma = 0.0114$ μm and for the linear controller is $\sigma = 0.0161$ μm. Hence, the adaptive controller reduces the standard deviation by about 30%.

The improvement due to the adaptive controller is also verified for the amplitude distribution of q (Fig. 8) by evaluating the normalized histogram of the sampled q-data. In addition to Section V-A, these data are another practical proof that the high-frequency amplitude peaks for the frequency response of the adaptive controller are artificially created by the special character of the tracking demand.

VI. Conclusion

An adaptive NN demand tracking controller has been applied to a VCM-actuator incorporating a solution for high-frequency resonance cancellation. This has been achieved by extending the linear control term of the NN-controller by notch-filters. Parameter overestimation was prevented by introducing a simple algorithm anti-windup technique into the adaptive control term. Practically, this approach has improved tracking behavior for

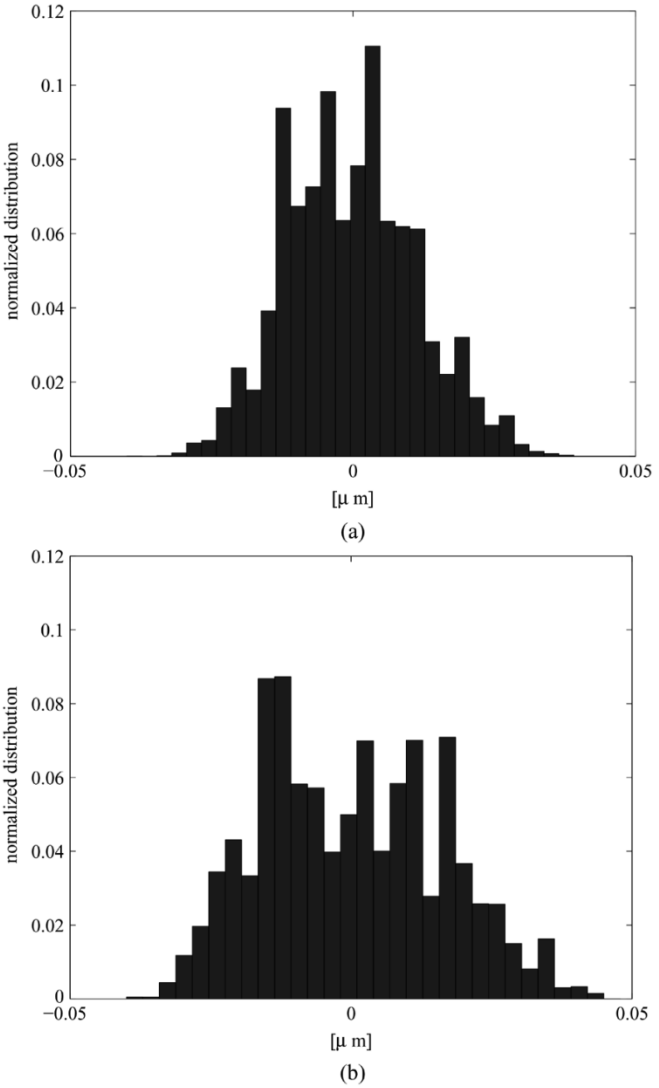

Fig. 8. Normalized histogram for tracking error for assessment of influence of rotating spindle (5000 rpm) and windage on the track following. (a) With both estimators enabled. (b) Linear control.

step demands and has reduced overshoots in comparison to the linear control term acting on its own. Sinusoidal demand signals can be reliably tracked for frequencies below 1.2 kHz. Furthermore, it has been shown that the adaptive controller can improve rejection of bias-forces and windage disturbances, which makes this controller a feasible track seeking and following controller.

For experimentation, up-to-date DSP-technology was used, making the implementation computationally intensive. The privilege of such an advanced experimental setup speeds up the prototyping of control system design. Nevertheless, microprocessor speeds in recent hard-disks have rapidly increased from a sampling frequency of 5 to nearly 20 kHz. This has allowed to implement new control techniques and more advanced methods, such as nonlinear adaptive techniques, have to be targeted in future using efficient assembly or C coding. For good performance and low number of NN-nodes, a major task of control design is the suitable and efficient choice of the radial basis functions. For track seeking, proper planning of the demand dynamics must be considered to prevent control signal saturation. All these questions shall be an area for future research.

REFERENCES

[1] R. Davies and S. K. Spurgeon, "Robust implementation of sliding mode control schemes," *Int. J. Syst. Sci.*, vol. 24, no. 4, pp. 773–743, 1993.
[2] P. Dupont, V. Hayward, B. Armstrong, and F. Altpeter, "Single state elastoplastic friction models," *IEEE Trans. Automat. Contr.*, vol. 47, no. 5, pp. 787–792, May 2002.
[3] K. Eddy, J. Steel, and W. Messner, "Bias in disk drive rotary actuators: Characterization, prediction, and compensation," *IEEE Trans. Magn.*, vol. 33, no. 3, pp. 2424–2436, May 1997.
[4] G. F. Franklin, J. D. Powell, and M. L. Workman, *Digital Control of Dynamic Systems*, 2nd ed. Reading, MA: Addison-Wesley, 1990.
[5] S. S. Ge, T. H. Lee, and C. J. Harris, *Adaptive Neural Network Control of Robotic Manipulators*, Singapore: World Scientific, 1998.
[6] S. S. Ge, T. H. Lee, and S. X. Ren, "Adaptive friction compensation of servo mechanisms," *Int. J. Syst. Sci.*, vol. 32, no. 4, pp. 523–532, 2001.
[7] T. B. Goh, Z. Li, B. M. Chen, T. H. Lee, and T. Huang, "Design and implementation of a hard disc drive servo using robust and perfect tracking approach," *IEEE Trans. Contr. Syst. Technol.*, vol. 9, no. 2, pp. 221–233, Mar. 2001.
[8] R. H. A. Hensen, M. J. G. van de Molengraft, and M. Steinbuch, "Frequency domain identification of dynamic friction model parameters," *IEEE Trans. Contr. Syst. Technol.*, vol. 10, no. 2, pp. 191–196, Mar. 2002.
[9] R. Horowitz and B. Li, "Adaptive track following servos for disk file actuators," *IEEE Trans. Magn.*, vol. 32, no. 3, pp. 1779–1786, May 1996.
[10] T. Huang, Y. Ding, S. Weerasooriya, and T. S. Low, "Disk drive pivot nonlinearity modeling and compensation through fuzzy logic," *IEEE Trans. Magn.*, vol. 34, no. 1, pp. 30–35, Jan. 1998.
[11] J. Ishikawa and M. Tomizuka, "Pivot friction compensation using an accelerometer and a disturbance observer for hard-disc drives," *IEEE/ASME Trans. Mechatron.*, vol. 3, no. 3, pp. 194–201, Sep. 1998.
[12] C. Kempf, W. Messner, M. Tomizuka, and R. Horowitz, "Comparison of four discrete-time repetitive control algorithms," *IEEE Control Syst. Mag.*, vol. 13, no. 6, pp. 48–54, Dec. 1993.
[13] M. Kobayashi, S. Nakagawa, T. Atsumi, and T. Yamaguchi, "High-bandwidth servo control designs for magnetic disc drives," in *Proc. 2001 IEEE/ASME Int. Conf. Advanced Intelligence Mechatronics*, 2001, pp. 1124–1129.
[14] S. Lewis, F. L. Jagannathan, and A. Yesildirek, *Neural Network Control of Robot Manipulators and Nonlinear Systems*. New York: Taylor & Francis, 1999.
[15] C.-J. Liou, S.-C. Lim, and Y.-Y. Chen, "Apply fuzzy seeking control to high precision hard disc driver," in *Proc. IEEE Int. Conf. Systems, Man and Cybernetics*, 1995, pp. 2472–2477.
[16] T. S. Liu and W. C. Wu, "Sliding mode-based learning control for positioning of flying pickup head," in *Proc. IEEE Int. Conf. Control Applications*, 2001, pp. 345–350.
[17] R. Oboe, A. Beghi, P. Capretta, and F. C. Soldavini, "Simulator for single stage and dual stage hard disc drives," in *Proc. 2001 IEEE/ASME Int. Conf. Advanced Intelligence Mechatronics*, 2001, pp. 1148–1152.
[18] N. Sadegh and R. Horowitz, "Stability and robustness analysis of a class of adaptive controllers for robotic manipulators," *Int. J. Robot. Res.*, vol. 9, no. 3, pp. 74–92, 1990.
[19] J.-J. E. Slotine and W. Li, *Applied Nonlinear Control*. Englewood Cliffs, NJ: Prentice-Hall, 1991.
[20] T.-J. Tarn, A. K. Bejczy, X. Yun, and Z. Li, "Effect of motor dynamics on nonlinear feedback robot arm control," *IEEE Trans. Robot. Automat.*, vol. 7, no. 1, pp. 114–122, Feb. 1991.
[21] F. Wang, T. Hurst, D. Abramovitch, and G. Franklin, "Disk drive pivot nonlinearity modeling part II: Time domain," in *Proc. Amer. Control Conf.*, Baltimore, MD, 1994, pp. 2604–2607.
[22] J. Wang, S. S. Ge, and T. H. Lee, "Adaptive friction compensation for servo mechanisms," in *Adaptive Control of Nonsmooth Dynamic Systems*, G. Tao and F. L. Lewis, Eds. Berlin, Germany: Springer, 2001, pp. 211–248.
[23] D. Wu, G. Guo, and T.-C. Chong, "Adaptive compensation of microactuator resonance in hard disc drives," *IEEE Trans. Magn.*, vol. 36, no. 5, pp. 2247–2250, Sep. 2000.
[24] D. Wu, G. Guo, and T. C. Chong, "Analysis and comparison of resonance compensation in dual-stage actuation system of HDDS," in *Proc. Amer. Control Conf.*, San Diego, CA, 2001, pp. 3824–3829.
[25] T. Yamaguchi, K. Shishida, S. Tohyama, and H. Hirai, "Mode switching control design with initial value compensation and its application to head positioning control on magnetic disk drives," *IEEE Trans. Ind. Electron.*, vol. 43, no. 1, pp. 65–73, Feb. 1996.